Applied Mathematics & Information Sciences
An International Journal

http://dx.doi.org/10.18576/amis/140619

New Accurate Approximation for the Sum of Generalized Gamma Distributions and its Applications

Toufik Chaayra[1,*], *Hussain Ben-azza*[1] *and Faissal El Bouanani*[2]

[1]ENSAM, Moulay Ismail University, Meknes, 15290, Morocco
[2]ENSIAS, Mohammed V University, Rabat, 10000, Morocco

Received: 8 Jul. 2020, Revised: 10 Oct. 2020, Accepted: 17 Oct. 2020
Published online: 1 Nov. 2020

Abstract: By considering the probability density function (PDF) of a generalized Gamma (GG) random variable (RV) evaluated in terms of a proper subset $H_{1,1}^{1,0}$ class of Fox's H-function (FHF) and the moment-based approximation to estimate the H-function parameters, a closed-form tight approximate expression for the distribution of the sum of independent and not necessarily identical GG distributed RVs is presented as well as a sufficient condition for the convergence is verified. Such proposed approximate PDF is useful analytical tool for analyzing the performance of L-branch maximal-ratio combining receivers subject to such a fading model. This result can be also of paramount importance when dealing with an intelligent reflecting surface subject to GG fading channels. Furthermore, various closed-form approximate expressions, such as the cumulative distribution function (CDF), moment-generating function, outage probability (OP), average channel capacity, nth moment of the signal-to-noise ratio (SNR), amount of fading, and average symbol error probability (ASEP) for numerous coherent digital modulation schemes, are derived and examined in terms of FHF. To gain further insight into the system performance, asymptotic closed-form expressions for the ASEP and OP are derived and interesting observations are made. Particularly, our asymptotic analysis reveals that the achievable diversity order for high SNR values depends essentially on the branches' number. The proposed mathematical analysis is assessed and corroborated by Monte-Carlo simulations using computer algebra systems, while the PDF and CDF are validated further with the aid of the Kullback-Leibler divergence criterion and Kolmogorov-Smirnov test, respectively.

Keywords: Average symbol error probability, Average channel capacity, Cumulative distribution function, Foxs H-function, Maximal-ratio combining, Moment-generating function, Probability density function, Sum of generalized Gamma random variables.

1 Introduction

The Fox's H-function is a Mellin-Barnes integral and first introduced by Fox [1] in 1961 as a symmetrical Fourier kernel, generalizing the well-known Meijer's G-function. Such integral is a complex contour integral involving a product of gamma functions. Due to its versatile nature, there have been various areas in astrophysics where FHF appears naturally, such as quantum mechanics issues concerning the computational solution of the one-dimensional space-time fractional, Schrödinger equations [2], analytic solar for the numerical solutions of the underlying system of differential equations and produce a simple mathematical model for the matter density distribution in the core of the sun, reaction-diffusion problems, the nuclear reaction rate theory [3], ...etc. Also, there have been applications to various wireless communication systems (WCSs) problems related to performance, commonly referred to as the H-distribution (HD). This function is characterized by significant flexibility in investigating the phenomenon of fading multipath channels as it generalizes various distributions [4].

Over recent years, numerous fading models have been proposed to characterize either fading or shadowing effects [5] accurately. Their use is evident in concrete as new communication technologies, such as massive multiple-input multiple-output (MIMO) communications, millimeter-wave (mmWave) communications, free-space optical (FSO) communications, as well as cognitive radios. Examples of these models include GG [6], Weibull and Nakagami-m distributions, among many others. Our work focuses on the application of the sum of

* Corresponding author e-mail: t.chaayra@edu.umi.ac.ma

independent and not necessarily identical (i.n.i.d) GG distributions and its application in WCSs subject to GG fading model. GG matches the fading gain attenuation in the radio-wave propagation subject to one-sided normal, Exponential, Rayleigh, Gamma, Nakagami-*m*, and Weibull distributions [6,7]. Towards this end, such distribution generalizes multiple fading models, e.g., Exponential, Rayleigh, Nakagami-*m*, Weibull, and other special cases, while it can also describe the Log-normal as a limiting case [8].

Leveraging the transforms of FHF known in the literature, various performance metrics of a communication system undergoing HD fading models, such as ASEP, OP, amount of fading (AoF), and average channel capacity (ACC) were investigated [4,5], [9]-[12].

Although the statistical properties for the product, quotient, and powers of HDs are known in the literature [13], the closed-form expression for the PDF of the sum of i.n.i.d HDs remains unknown. This problem plays a prominent role in statistical performance analysis of WCSs, such as examinating the performance of famous diversity techniques, namely equal-gain combining (EGC), and maximal-ratio combining (MRC), known to be the optimum combiner for various system configuration [5].

To this end, the distribution of the sum of HD RVs is required to tackle the performance of the aforementioned receivers. That sum can be approximated using (i) Bodenschatz's methods [14], and (ii) moment-based approximation estimating FHF's parameters [15]. Particularly, the sum of HDs has been developed for convergent type *VI* FHF variates [16], relying on the three first moments of the RVs' sum.

It is worth mentioning that diversity technique is a very effective method to overcome the fading's problem, in which the received signals at each receiver's antenna are combined and weighted appropriately to improve the WCS' performance. The multiple copies of the signal, sent by the transmitter and arriving at the receiver from multiple paths due to numerous optical phenomenons, e.g. diffraction, reflection, scattering, and shadowing, can be combined efficiently with the help of well-known diversity techniques in the literature.

Various works that addressed performance of diversity receivers over uncorrelated GG fading channels have been investigated [17]-[23]. The authors in [17] have presented the performance of *M*-ary modulation schemes for MRC, EGC, and SC, whereas in [18], switch-and-stay combining over i.n.i.d GG fading channels has been investigated. The moments of the output SNR at MRC and EGC receivers, under i.n.i.d fading channels, are derived in [19]. Average bit error rate (ABER) expressions for binary digital modulation schemes experiencing GG fading model were investigated in [20]. A unified analysis of ASEP for a general class of *M*-ary modulation schemes with MRC and post-detection EGC over GG fading channels has been addressed in [21]. Considering the product of *N* GG RVs, the authors in [22, 23] have proposed the use of union upper bounds for the distribution of the sum of GG RVs in closed-form, based on which, the OP and the ABEP of EGC receivers over GG fading channel are analyzed.

Motivated by the aforementioned discussion, our main contributions are summarized, as follows:

(i) We propose, based on the moments' method, a novel closed-form approximate expressions of the sum of i.n.i.d GG distributed RVs,
(ii) We verify a sufficient condition for the convergence of the analytical approximate PDF using the sum of $H_{1,1}^{1,0}$ type *VI* convergent FHF [16],
(iii) Based on the above-mentioned result, we derive some performance metrics, namely OP, AoF, ACC, ASEP for various coherent *M*-ary modulation schemes and MRC receiver experiencing i.n.i.d GG fading channels. These results are valid for any operating scenarios to an arbitrary receiver branches' number and GG shape parameters' values,
(iv) We prove and validate tightness of the approximate analytical expressions through Monte-Carlo simulations. Moreover, accuracy of approximate PDF and CDF were validated via the Kullback-Leibler divergence (KLD) criteria and the Kolmogorov-Smirnov (KS) statistical test, respectively,
(v) We investigate the asymptotic expressions for ASEP and OP at high SNR values and we demonstrate that the achievable diversity order is related to the approximate PDF parameter, Φ, which depends basically on the branches' number.

The remainder of this paper is structured, as follows: In Section 2, we present preliminaries as mathematical tools on GG distribution and HD including sufficient convergence conditions. Section 3 summarizes new tight approximate expressions for PDF, CDF, and moment-generating function (MGF) of i.n.i.d GG RVs sums in terms of FHF. As an application, numerous performance metrics' approximate expressions of a WCS employing MRC receiver and undergoing i.n.i.d multipath GG fading channels are presented in Section 4. Section 5 depicts simulation results and provides some insights on the system performance. Finally, closing remarks that summarize the current contributions are reported in Section 6.

2 Mathematical Prerequisites

In this section, we provide the statistical characteristic of GG distribution along with its properties. Next, we present the convergence conditions of the type *VI* FHF [16] and the connected concept of Mellin transforms relevant to this contribution.

Table 1: Mathematical notations.

Notation	Meaning
$\Gamma(.)$	Euler Gamma function [24, Eq. (6.1.1)]
$\mathbb{E}[.]$	Expectation operator
μ_r	rth moment
$\mathbb{V}[.]$	Variance function
$Q(.)$	Gaussian Q-function [24, Eq. (26.2.3)]
$H[.]$	Fox's H-function [13, Eq. (6.2.1)]
$\mathscr{C}$	Infinite contour integral in the complex plane
$\mathscr{H}(.)$	Integrand of Mellin-Barnes integral of $H[.]$
$\mathscr{M}_s\{.\}$	Mellin transform of $H[.]$ [13, Eq. (2.8.9)]
$\mathscr{M}_z^{-1}\{.\}$	Inverse Mellin transform [13, Eq. (2.8.10)]
$\mathbb{R}^+$	Set of non-negative real numbers $[0,\infty)$
$f_Z(.)$	Probability density function of GG RV Z
$F_Z(.)$	Cumulative density function of GG RV Z
$Z\sim \mathrm{GG}(.,.,.)$	Z is GG distributed
$\overline{P}_s$	Average symbol error probability

2.1 Notations

2.2 Generalized Gamma distribution

Definition 2.1. Let $\{Z_i\}_{1\le i\le N}$ be the family of three-parameters GG distribution; each Z_i is denoted by $\mathrm{GG}(m_i,\beta_i,\Omega_i)$. Its PDF is given by [25, Eq. (1)]

$$f_{Z_i}(z)=\frac{\beta_i}{\Omega_i\Gamma(m_i)}\left(\frac{z}{\Omega_i}\right)^{m_i\beta_i-1}\exp\left[-\left(\frac{z}{\Omega_i}\right)^{\beta_i}\right], \quad (1)$$

where m_i and β_i are the shape parameters, while Ω_i is the scale parameter.

Property 2.1. (nth moment) Let's define the function $d_k(x,y)=\frac{\Gamma(x+k/y)}{\Gamma(x)}$. If $Z_i\sim \mathrm{GG}(m_i,\beta_i,\Omega_i)$, then the nth moment can be expressed as [25, Eq. (3)]

$$\mathbb{E}[Z_i^n]=\Omega_i^n d_n(m_i,\beta_i). \quad (2)$$

Remark 2.1. If Z_i is GG distributed, then its variance can be evaluated using (2), as

$$\mathbb{V}[Z_i]=\Omega_i^2\left(d_2(m_i,\beta_i)-d_1^2(m_i,\beta_i)\right).$$

Moreover, it is noticeable from the PDF given in (1) generalizes that of (i) exponential RV if $m=\beta=1$, (ii) Nakagami-m RV when $\beta=1$, (iii) Weibull RV if $m=1$, (iv) Log-normal RV when $m\to\infty$. Furthermore, by setting $\beta=2$, we obtain a subfamily of GG, known as the generalized normal (GN) distribution, which is a flexible family and includes half-normal, Rayleigh, and Maxwell-Boltzmann RVs when $m=1/2,\ 1,\ 3/2$, respectively [27].

Property 2.2. If $Z\sim \mathrm{GG}(m,\beta,\Omega)$, then [25, Eq. (2)]

$$Z^n\sim \mathrm{GG}\left(m,\frac{\beta}{n},\Omega^n\right),\ n>0.$$

2.3 H-distribution

Definition 2.2. The Fox's H-function is defined via the Mellin-Barnes type integral as [13, Eq. (6.2.1)]

$$H[z]\triangleq H_{p,q}^{m,n}\left[z\left|\begin{matrix}(a_i,A_i)_{1,p}\\(b_i,B_i)_{1,q}\end{matrix}\right.\right]=\frac{1}{2\pi j}\int_{\mathscr{C}_s}\mathscr{H}(s)z^{-s}ds,$$

where $j=\sqrt{-1}$, $z\neq 0$, and

$$\mathscr{H}(s)=\frac{\prod_{i=1}^{m}\Gamma(b_i+B_is)\prod_{i=1}^{n}\Gamma(1-a_i-A_is)}{\prod_{i=m+1}^{q}\Gamma(1-b_i-B_is)\prod_{i=n+1}^{p}\Gamma(a_i+A_is)},$$

is the Mellin transform of the FHF. An empty product is interpreted as unity; $m,n,p,q\in\mathbb{N}$ with $0\le n\le p$, $0\le m\le q$, $a_i,b_i\in\mathbb{C}$, $A_i\in\mathbb{R}^+$ $(i=1,...,p)$, $B_i\in\mathbb{R}^+$ $(i=1,...,q)$, and $\mathscr{C}_s$ is an infinite contour in the complex s-plane, keeping the poles

$$b_{il}=-\frac{b_i+l}{B_i},\ (i=1,...,m;\ l=0,1,2,...);$$

of the Gamma functions $\Gamma(b_i+B_is)$, placed on the left side of $\mathscr{C}_s$, separated from the poles

$$a_{ik}=\frac{1-a_i+k}{A_i},\ (i=1,...,n;\ k=0,1,2,...);$$

of the Gamma functions $\Gamma(1-a_i-A_is)$, located on the right side of $\mathscr{C}_s$.

Definition 2.3. The FHF $H[z]$ is called of type VI if the following conditions are satisfied [16, p. 72]

$$D\ge 0,\ E=0,\ F<0,$$

with

$$\begin{cases} D=\sum_{i=1}^{n}A_i+\sum_{i=1}^{m}B_i-\sum_{i=n+1}^{p}A_i-\sum_{i=m+1}^{q}B_i\\ E=\sum_{i=1}^{p}A_i-\sum_{i=1}^{q}B_i\\ F=\Re\left(\sum_{i=1}^{q}b_i-\sum_{i=1}^{p}a_i+\frac{p}{2}-\frac{q}{2}\right)\end{cases}.$$

where $\Re(.)$ denotes the real part of a complex number.

The type VI FHF can be evaluated as the positive sum of LHP residues, the negative sum of RHP residues, or

both, depending on the value of the argument z restricted to $|\arg(z)| < \min(\pi, \pi\frac{D}{2})$. We have

$$H[z] = \begin{cases} \sum_i z_i^{(L)}, \ |z| < \dfrac{1}{\varsigma} \\ -\sum_i z_i^{(R)}, \ |z| > \dfrac{1}{\varsigma} \\ \sum_i z_i^{(L)} = -\sum_i z_i^{(R)}, \ |z| = \dfrac{1}{\varsigma} \text{ and } F < -1 \end{cases},$$

where $\varsigma = \prod_{i=1}^{p} A_i^{A_i} \prod_{i=1}^{q} B_i^{-B_i}$ with $z_i^{(L)}$ and $z_i^{(R)}$ denote, respectively, the residue corresponding to the ith pole located in the left half-plane (LHP) and the right half-plane (RHP), respectively.

Property 2.3. For any positive number α, the following relation holds [14, Eq. (2.45)]

$$\frac{2\sqrt{\pi}}{4^{b_1}} H_{p+1,q}^{m,n}\left[4^{B_1}\alpha z \left| \begin{matrix} (a_i, A_i)_{1,p}, (b_1+\frac{1}{2}, B_1) \\ (2b_1, 2B_1), (b_i, B_i)_{2,q} \end{matrix} \right.\right] = H[\alpha z]. \tag{3}$$

Definition 2.4. The Mellin Transform of $H[\alpha z]$ is defined on $[0,\infty)$ as [13, Eq. (6.2.9)],

$$\begin{aligned} \mathscr{M}_s\{H[\alpha z]\} &= \int_0^\infty H[\alpha z] z^{s-1} dz \\ &= \alpha^{-s} \mathscr{H}(s), \end{aligned} \tag{4}$$

where $s \in \mathbb{C}$, while its inverse Mellin transform is given by

$$\mathscr{M}_z^{-1}\{\alpha^{-s}\mathscr{H}(s)\} = H[\alpha z].$$

Definition 2.5. (H-distribution) The HD is a RV with PDF of the form [13, Eq. (6.3.1)]

$$f_Z(z) = \begin{cases} \kappa H_{p,q}^{m,n}\left[\alpha z \left| \begin{matrix} (a_i, A_i)_{1,p} \\ (b_i, B_i)_{1,p} \end{matrix} \right.\right], & z, \alpha, \kappa > 0, \\ 0, & \text{otherwise}, \end{cases}$$

where α and the constant κ are chosen such that $\int_0^\infty f_Z(z)dz = 1$.

Property 2.4. (Raw Moments) Considering that a real-valued RV Z can be represented as an HD, the nth moment of Z is easily obtained using the Mellin transform as [13, Eq. (6.3.3b)]

$$\begin{aligned} \mu_n &= \mathbb{E}[Z^n] \\ &= \mathscr{M}_{n+1}\{f_Z(z)\} \\ &= \frac{\kappa \mathscr{H}(n+1)}{\alpha^{n+1}}. \end{aligned} \tag{5}$$

3 Novel approximate HD for the sum of i.n.i.d GG RVs

Lemma 3.1. Let $\{Z_i\}_{1\le i\le N}$ be N i.n.i.d GG(m_i, β_i, Ω_i) RVs. The PDF of Z_i can be expressed as a FHF

$$f_{Z_i}(z) = \frac{1}{\Omega_i \Gamma(m_i)} H_{0,1}^{1,0}\left[\frac{z}{\Omega_i} \left| \begin{matrix} -;- \\ \left(m_i - \frac{1}{\beta_i}, \frac{1}{\beta_i}\right); - \end{matrix} \right.\right], \ z \ge 0 \tag{6}$$

Proof. By rewriting the exponential function as an FHF [13, Eq. (6.2.5)]

$$\begin{aligned} \exp\left\{-\left(\frac{z}{\Omega_i}\right)^{\beta_i}\right\} &= H_{0,1}^{1,0}\left[\left(\frac{z}{\Omega_i}\right)^{\beta_i} \left| \begin{matrix} -;- \\ (0,1); - \end{matrix} \right.\right] \\ &= \frac{1}{2\pi j}\int_{\mathscr{C}_s} \Gamma(s)\left(\frac{z}{\Omega_i}\right)^{-\beta_i s} ds, \end{aligned} \tag{7}$$

and substituting (7) into (1) along with performing some computations, we get

$$f_{Z_i}(z) = \frac{\beta_i}{\Omega_i \Gamma(m_i)} \frac{1}{2\pi j}\int_{\mathscr{C}_s} \Gamma(s)\left(\frac{z}{\Omega_i}\right)^{\beta_i(m_i-s)-1} ds.$$

Finally, using the change of variable $t = \beta_i(s-m_i)+1$, (6) is obtained, which concludes the proof of **Lemma 3.1**.

Property 3.1. The $H_{0,1}^{1,0}$ FHF can be written as an $H_{1,1}^{1,0}$ FHF, as follows:

$$\begin{aligned} H_{0,1}^{1,0}\left[\frac{z}{\alpha_i} \left| \begin{matrix} -;- \\ \left(m_i - \frac{2}{\beta_i}, \frac{2}{\beta_i}\right); - \end{matrix} \right.\right] &= \frac{2\sqrt{\pi}}{4^{m_i - \frac{2}{\beta_i}}} \\ \times H_{1,1}^{1,0}\left[4^{\frac{2}{\beta_i}}\frac{z}{\alpha_i} \left| \begin{matrix} -; \left(m_i - \frac{2}{\beta_i} + \frac{1}{2}, \frac{2}{\beta_i}\right) \\ \left(2m_i - \frac{4}{\beta_i}\right), \frac{4}{\beta_i}\right); - \end{matrix} \right.\right], \ z \ge 0. \end{aligned}$$

Proof. Using (3), the $H_{0,1}^{1,0}$ FHF given in (6) can be written as an $H_{1,1}^{1,0}$ FHF as shown in *Property 3.1.*

The following Lemma presents an approximation of the PDF of the sum of i.n.i.d HDs relying on the moments-based approximation method [14, 15].

Lemma 3.2. The PDF of $Z = \sum_{i=1}^{N} Z_i$ can be approximated by a FHF as

$$f_Z(z) \approx a H_{1,1}^{1,0}\left[\frac{z}{\lambda} \left| \begin{matrix} -;(b,1) \\ (c,1); - \end{matrix} \right.\right], \ z \ge 0 \tag{8}$$

where λ is any arbitrary positive number, and

$$\begin{aligned} a = \frac{\Gamma(b+1)}{\lambda\Gamma(c+1)}, \ b = \frac{\mu_1\lambda - \mu_2}{\mu_2 - \mu_1^2} - 1, \\ c = \left(\frac{\mu_1\lambda - \mu_2}{\mu_2 - \mu_1^2}\right)\frac{\mu_1}{\lambda} - 1. \end{aligned} \tag{9}$$

Furthermore, this PDF converges if the real parameter λ verifies

$$\lambda < \mu_1 \text{ or } \lambda > \frac{\mu_2}{\mu_1}, \tag{10}$$

where μ_1 and μ_2 are the first and the second moment of Z.

Proof. The PDF of the sum of type VI convergent HD Z_i can be approximated by an FHF, as follows [14, p. 140]

$$\begin{aligned} f_Z(z) &\approx a H_{1,1}^{1,0}\left[\frac{z}{\lambda}\middle|\begin{matrix}-;(b,1)\\(c,1);-\end{matrix}\right] \\ &= \frac{a}{2\pi j}\int_{\mathscr{C}_s}\frac{\Gamma(c+s)}{\Gamma(b+s)}\left(\frac{z}{\lambda}\right)^{-s}ds, \end{aligned}$$

where for an arbitrary chosen positive number, λ, a, b, and c are the solutions of the following non-linear system of equations obtained from (5),

$$\mu_n = a\lambda^{n+1}\frac{\Gamma(c+n+1)}{\Gamma(b+n+1)},\ n=0,1,2.$$

Now, using $\mu_0 = 1$, along with [24, Eq. (6.1.15)], (9) can be straightforwardly obtained.

Further, relying on (2), the expectation of Z can be expressed as

$$\mu_1 = \sum_{i=1}^{N}\Omega_i d_1(m_i,\beta_i),$$

while the second moment yields using the multinomial theorem as

$$\mu_2 = \sum_{i=1}^{N}\Omega_i^2 d_2(m_i,\beta_i) + 2\sum_{i=1}^{N-1}\sum_{l=i+1}^{N}\Omega_i\Omega_l d_1(m_i,\beta_i)\,d_1(m_l,\beta_l).$$

Note that a sufficient condition for the convergence of the FHF given in (8) is $c-b<0$. Thus, as $\mu_2-\mu_1^2>0$, it follows that the sign of $c-b$ is that of $\left(\mu_1-\frac{\mu_2}{\lambda}\right)(\mu_1-\lambda)$, and then any arbitrary value of λ greater than $\frac{\mu_2}{\mu_1}$ or less than μ_1 can be chosen, which concludes the proof of **Lemma 3.2.**

Corollary 3.1. The type VI FHF, given in (8), converges if

$$\lambda > \triangle,\ \forall z \geq 0, \tag{11}$$

with

$$\triangle = \frac{\mu_2}{\mu_1}\left(1+\sqrt{1-\frac{\mu_1^2}{\mu_2}}\right).$$

Proof. If $c-b+1<0$, we can use the sum of either LHP or RHP residues at $z=\lambda$. Moreover,

$$c-b+1 = -\frac{\mu_1\lambda^2 - 2\mu_2\lambda + \mu_1\mu_2}{\lambda\left(\mu_2-\mu_1^2\right)}.$$

That is, as $\mu_2-\mu_1^2>0$, any value of λ greater than $\triangle$ can be chosen to have $c-b+1<0$. Because $\triangle > \frac{\mu_2}{\mu_1}$, the PDF given in (8) converges for any value of z if $\lambda > \triangle$. That concludes the proof of **Corollary 3.1.**

Given that the PDF of the sum RVs, given in (8), exists if the conditions $\lambda > \mu_2/\mu_1$ of (10) and/or (11) are achieved, and that the greater λ is, the more accurate such an approximation is [26]. Furthermore, handling large values of λ leads to a computation instability, particularly when using Mathematica/Matlab predefined in-routines. To this end, it can be deduced that this expression can be further approximated for large values of λ. Consequently, to get the asymptotic expression, the parameter λ in PDF expression will be next eliminated by evaluating the limit of (8) as λ tends to infinity.

Theorem 3.1. If $\{Z_i\}_{1\leq i\leq N}$ are i.n.i.d GG variates with PDFs $f_{Z_i}(z)$, given in (6), then the PDF of $Z=\sum_{i=1}^{N}Z_i$ can be approximated as

$$f_Z(z) \approx \frac{\Psi}{\Gamma(\Phi)}H_{0,1}^{1,0}\left[\Psi z\middle|\begin{matrix}-;-\\(\Phi-1,1);-\end{matrix}\right], \tag{12}$$

where

$$\Phi = \frac{\mu_1^2}{\mu_2-\mu_1^2},\ \Psi = \frac{\mu_1}{\mu_2-\mu_1^2}.$$

Proof. Reproducing (8), one gets

$$\begin{aligned} f_Z(z) &\approx \frac{\Gamma(b+1)}{\lambda\Gamma(c+1)}H_{1,1}^{1,0}\left[\frac{z}{\lambda}\middle|\begin{matrix}-;(b,1)\\(c,1);-\end{matrix}\right] \\ &= \frac{\Gamma(b+1)}{\lambda\Gamma(c+1)}\frac{1}{2\pi j}\int_{\mathscr{C}_s}\frac{\Gamma(c+s)}{\Gamma(b+s)}\left(\frac{z}{\lambda}\right)^{-s}ds \\ &= \frac{1}{2\pi j\lambda}\int_{\mathscr{C}_s}\frac{\Gamma(c+s)}{\Gamma(c+1)}\frac{\Gamma(b+1)\lambda^s}{\Gamma(b+s)}z^{-s}ds, \end{aligned} \tag{13}$$

where

$$b = \left(\lambda-\frac{\mu_2}{\mu_1}\right)\Psi - 1,\ \ c = \Phi - \frac{\mu_2\Psi}{\lambda} - 1. \tag{14}$$

From (14), we have

$$\frac{\Gamma(c+s)}{\Gamma(c+1)} \sim \frac{\Gamma(\Phi-1+s)}{\Gamma(\Phi)} \text{ as } \lambda\to+\infty.$$

On the other side, employing the Stirling's relation [24, Eq. (6.1.39)] yields

$$\frac{\Gamma(b+1)\lambda^s}{\Gamma(b+s)} \sim \lambda\Psi^{-s+1} \text{ as } \lambda\to+\infty.$$

Thus,

$$\frac{1}{\lambda}\frac{\Gamma(c+s)}{\Gamma(c+1)}\frac{\Gamma(b+1)\lambda^s}{\Gamma(b+s)}z^{-s} \sim \frac{\Gamma(\Phi-1+s)}{\Gamma(\Phi)}\Psi^{-s+1}z^{-s},$$
$$\text{as } \lambda\to+\infty.$$

It follows that equation (13) becomes

$$f_Z(z) \approx \frac{\Psi}{\Gamma(\Phi)} \frac{1}{2\pi j} \int_{\mathscr{C}_s} \Gamma(\Phi - 1 + s) (\Psi z)^{-s} ds, \quad (15)$$

which concludes the proof of **Theorem 3.1.**

Corollary 3.2. The CDF of $Z = \sum_{i=1}^{N} Z_i$ can be accurately approximated as

$$F_Z(z) \approx \frac{1}{\Gamma(\Phi)} H_{1,2}^{1,1} \left[\Psi z \middle| \begin{matrix} (1,1); - \\ (\Phi,1); (0,1) \end{matrix} \right]. \quad (16)$$

Proof. The CDF of Z is straightforwardly derived from its PDF given in (8) as

$$\begin{aligned} F_Z(z) &= \mathrm{P}(Z \leq z) \\ &= \int_0^z f_Z(x) dx \\ &\approx \frac{\Psi}{\Gamma(\Phi)} \frac{1}{2\pi j} \int_{\mathscr{C}_s} \Gamma(\Phi - 1 + s) \Psi^{-s} \left(\int_0^z x^{-s} dx \right) ds \\ &= \frac{\Psi}{\Gamma(\Phi)} \frac{1}{2\pi j} \int_{\mathscr{C}_s} \frac{\Gamma(\Phi - 1 + s)}{-s+1} \Psi^{-s} z^{-s+1} ds. \end{aligned}$$

Then, using [24, Eq. (6.1.15)] alongside with performing some simple algebraic manipulations, and using a linear change of variable $t = s - 1$, the CDF can be reduced to

$$F_Z(z) \approx \frac{1}{\Gamma(\Phi)} \frac{1}{2\pi j} \int_{\mathscr{C}_s} \frac{\Gamma(\Phi + s)\Gamma(-s)}{\Gamma(1-s)} (\Psi z)^{-s} ds.$$

Thus, the proof of **Corollary 3.2.** is concluded.

Proposition 3.1. Suppose that $\{Z_i\}_{1 \leq i \leq N}$ are N i.n.i.d GG(m_i, β_i, Ω_i) RVs. The MGF, $M_Z(x)$, of $Z = \sum_{i=1}^{N} Z_i$ can be tightly approximated as

$$M_Z(x) \approx \frac{1}{\Gamma(\Phi)} H_{1,1}^{1,1} \left[-\frac{\Psi}{x} \middle| \begin{matrix} (1,1); - \\ (\Phi,1); - \end{matrix} \right], \forall x < 0. \quad (17)$$

Proof. The MGF of Z is defined as

$$M_Z(x) \triangleq \mathbb{E}\left[e^{xZ}\right], \; x \leq 0.$$

From (12), the MGF can be approximated in terms of the Mellin transform as

$$\begin{aligned} M_Z(x) \approx & \frac{\Psi}{\Gamma(\Phi)} \frac{1}{2\pi j} \int_{\mathscr{C}_s} \Gamma(\Phi - 1 + s) \Psi^{-s} \\ & \times \mathscr{M}_{1-s} \left(H_{0,1}^{1,0} \left[-xz \middle| \begin{matrix} -; - \\ (0,1); - \end{matrix} \right] \right) ds. \end{aligned} \quad (18)$$

Since $x \leq 0$, the Mellin transform of the FHF is

$$\mathscr{M}_{1-s} \left(H_{0,1}^{1,0} \left[-xz \middle| \begin{matrix} -; - \\ (0,1); - \end{matrix} \right] \right) = (-x)^{s-1} \Gamma(1-s). \quad (19)$$

Now, substituting (19) into (18), we have

$$\begin{aligned} M_Z(x) \approx & \frac{1}{\Gamma(\Phi)} \frac{1}{2\pi j} \int_{\mathscr{C}_s} \Gamma(\Phi - 1 + s) \Gamma(1-s) \\ & \times \left(-\frac{\Psi}{x} \right)^{-s+1} ds. \end{aligned} \quad (20)$$

Hence, by performing the change of variable $t = s - 1$, the MGF of Z will be expressed as given in (17), which concludes the proof of **Proposition 3.1.**

4 Applications to WCS

In this section, numerous performance metrics of a WCS employing MRC receiver and experiencing uncorrelated GG fading multipath channels are investigated relying on the previous proposed PDF approximation.

4.1 System Model

Let us consider an L-branch MRC receiver operating over i.n.i.d GG fading multipath channels. The received signal, r_i, at its ith antenna is expressed as [23]

$$r_i = g_i x + n_i, \; (i = 1, \ldots, L)$$

where x is the complex transmitted symbol, with $\mathbb{E}[|x|^2] = E_s$ being the transmitted average symbol energy, $g_i = R_i e^{j\psi_i}$ $(i = 1, \ldots, L)$ where R_i is the instantaneous fading amplitude corresponding to the received signals on the ith branch, assumed being i.n.i.d GG(m_i, β_i, Ω_i) distributed, ψ_i is the corresponding instantaneous phase, while n_i refers to the instantaneous additive white Gaussian noise (AWGN) with zero mean and single-sided power spectral density $N_0 = \mathbb{E}[n_i^2]$, assumed to be identical for all branches. Moreover

- $\beta_i > 0$ and $m_i > 0$ are two parameters related to the fading severity. As m and/or β_i increases, the ith channel becomes more reliable,
- Ω_i is related to the average fading power $\mathbb{E}[R_i^2]$ and the Gamma function. Substituting $\mathbb{E}[R_i^2]$ into (2) yileds

$$\Omega_i = m_i \left[\frac{\mathbb{E}[R_i^2]}{d_2(m_i, \beta_i)} \right]^{\frac{\beta_i}{2}}.$$

If each branch is weighted by w_i, then the linear combination of the received signals at the receiver's output, as shown in Fig. 1, is expressed as

$$\begin{aligned} r &= \sum_{i=1}^{L} w_i r_i \\ &= \sum_{i=1}^{L} w_i g_i x + \sum_{i=1}^{L} w_i n_i. \end{aligned}$$

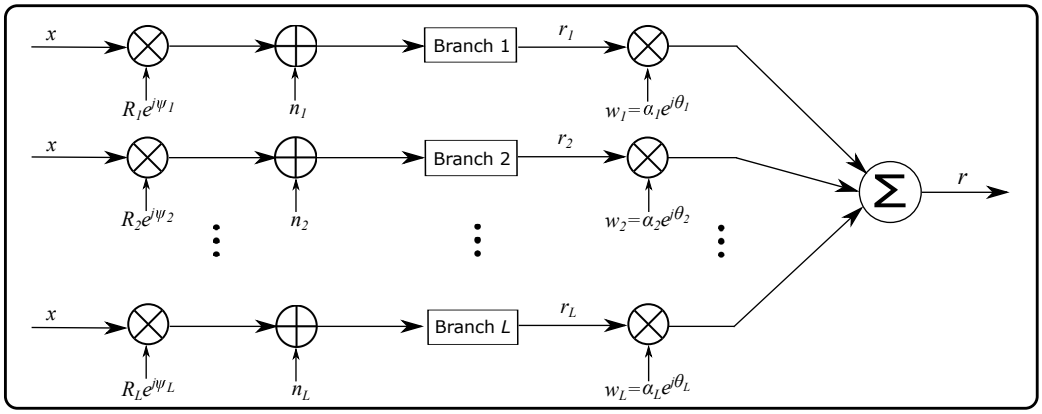

Fig. 1: The MRC system model.

Therfore, the output's SNR, γ, is given by

$$\gamma = \frac{\left|\sum_{i=1}^{L} w_i g_i x\right|^2}{\sum_{i=1}^{L} |w_i n_i|^2} = \frac{E_s \left|\sum_{i=1}^{L} w_i g_i\right|^2}{N_0 \sum_{i=1}^{L} |w_i|^2}, \tag{21}$$

Using Cauchy-Schwartz inequality in the numerator of (21), we obtain

$$\gamma \leq \frac{E_s \left(\sum_{i=1}^{L} |w_i|^2\right)\left(\sum_{i=1}^{L} |g_i|^2\right)}{N_0 \sum_{i=1}^{L} |w_i|^2},$$

which maximizes if the weights w_i are taken such that $w_i = g_i^*$, $\forall i \in \{1,\ldots,L\}$.
Thus, the resulting combiner SNR becomes

$$\gamma = \sum_{i=1}^{L} \frac{E_s}{N_0}|g_i|^2 = \sum_{i=1}^{L} \frac{E_s}{N_0} R_i^2 = \sum_{i=1}^{L} \gamma_i,$$

where the instantaneous SNR per symbol at the ith diversity channel is

$$\gamma_i = \frac{E_s}{N_0} R_i^2. \tag{22}$$

Further, the average of γ_i can be obtained from (22)

$$\overline{\gamma}_i = \frac{E_s}{N_0}\mathbb{E}[R_i^2] = \frac{E_s}{N_0} d_2(m_i,\beta_i)\left(\frac{\Omega_i}{m_i}\right)^{2/\beta_i}.$$

Note that if R_i are i.i.d., then $\overline{\gamma}_i = \overline{\gamma}_1$, $\forall i$.

Furthermore, using (2), the nth moment of R_i can be expressed as

$$\mu_n^{(R_i)} = \mathbb{E}[R_i^n] = d_n(m_i,\beta_i)\left(\frac{\Omega_i}{m_i}\right)^{n/\beta_i}.$$

4.2 Statistical Analysis

In this subsection, various metrics related to the performance of the considered WCS are approximated and their asymptotic expressions in high SNR regime are deduced.

4.2.1 nth moment of the output SNR

The nth moment of γ is by definition $\mu_n \triangleq \mathbb{E}[\gamma^n]$. By applying (12), the nth moment of the MRC output SNR undergoing i.n.i.d GG fading channels can be approximated as

$$\mu_n = \mathscr{M}_{n+1}\left[f_\gamma(\gamma)\right] \approx \frac{1}{\Psi^n}\frac{\Gamma(\Phi+n)}{\Gamma(\Phi)}. \tag{23}$$

4.2.2 Amount of Fading

The AoF, defined as the ratio of the variance to the square average SNR per symbol, i.e., $\eta_\gamma = \frac{\mathbb{V}[\gamma]}{\overline{\gamma}^2}$, is a unified

measure of the fading severity, which is typically independent of the average fading power [5, Eq. (1.27)]

$$\eta_\gamma = \frac{\mu_2}{\mu_1^2} - 1.$$

For AWGN channel, $\eta_\gamma = 0$, which means that the smaller η_γ is, the better the channel is. Then the system performance improves.

Now, having the two moments μ_1 and μ_2 of γ from (23), and using [24, Eq. (6.1.15)] we get

$$\begin{aligned}\eta_\gamma &= \frac{\frac{1}{\Psi^2}\frac{\Gamma(\Phi+2)}{\Gamma(\Phi)}}{\frac{1}{\Psi^2}\frac{\Gamma^2(\Phi+1)}{\Gamma^2(\Phi)}} - 1 \\ &= \frac{1}{\Phi}. \end{aligned} \tag{24}$$

4.2.3 Outage probability of the output SNR γ

Let γ_{min} denote the minimum SNR threshold that guarantees the reliable communication and having the corresponding channel not in outage.

A. Approximate analysis

Corollary 4.1. The outage probability, P_{out}, can be approximated as

$$P_{out} \approx \frac{1}{\Gamma(\Phi)} H_{1,2}^{1,1}\left[\Psi\gamma_{min}\middle|\begin{matrix}(1,1);-\\(\Phi,1);(0,1)\end{matrix}\right], \tag{25}$$

where

$$\Phi = \frac{\overline{\gamma}^2}{\mu_2 - \overline{\gamma}^2},\ \Psi = \frac{\overline{\gamma}}{\mu_2 - \overline{\gamma}^2}. \tag{26}$$

Proof. For a minimum SNR threshold γ_{min}, the OP is defined as $P_{out} = F_\gamma(\gamma_{min})$ [5, Eq. (1.4)]. Thus, (25) can be seen from (16).

B. Asymptotic Behavior

Property 4.1. In the high SNR regime, OP can be asymptotically approximated as

$$P_{out} = \frac{(\gamma_{min}\Phi)^\Phi}{\Gamma(\Phi+1)}\overline{\gamma}^{-\Phi} + o\left(\overline{\gamma}^{-\Phi}\right). \tag{27}$$

Proof. According to [32, Theorem 1.11], when $\overline{\gamma}$ tends to infinity, $\gamma_{min}\Psi$ approaches zero. Hence, we use the residue of the associated integrand of (16) at the simple poles $-\Phi-k$ of $\Gamma(\Phi+s)$, where k is a natural number, belonging to LHP of the contour $\mathscr{C}_s$ as

$$\begin{aligned}&\operatorname*{Res}_{s=-\Phi-k}\left[\frac{\Gamma(\Phi+s)\Gamma(-s)}{\Gamma(1-s)}(\gamma_{min}\Psi)^{-s}\right] \\ &= \lim_{s\to-\Phi-k}\frac{(s+\Phi+k)\Gamma(\Phi+s)\Gamma(-s)}{\Gamma(1-s)}(\gamma_{min}\Psi)^{-s}.\end{aligned}$$

Using the identity $\Gamma(z+1) = z\Gamma(z)$, and

$$\begin{aligned}\operatorname*{Res}_{s=-k}\Gamma(s) &= \lim_{s\to-k}(s+k)\Gamma(s) \\ &= \frac{(-1)^k}{k!},\ (k=0,1,2,\ldots)\end{aligned}$$

we have

$$\operatorname*{Res}_{s=-\Phi-k}\left[\frac{\Gamma(\Phi+s)\Gamma(-s)}{\Gamma(1-s)}(\gamma_{min}\Psi)^{-s}\right] = \frac{(-1)^k(\gamma_{min}\Psi)^{\Phi+k}}{k!(\Phi+k)}. \tag{28}$$

From (26), we get

$$\Psi = \frac{\Phi}{\overline{\gamma}}. \tag{29}$$

Lastly, substituting (29) into (28), one obtains (27), which concludes the proof of *Property 4.1.*

4.2.4 Average channel capacity

Property 4.2. Let B_w be the channel bandwidth. The ACC under MRC diversity and i.n.i.d GG fading channels can be approximated as

$$\overline{C} \approx \frac{\Psi B_w}{\Gamma(\Phi)\ln(2)} H_{2,3}^{3,1}\left[\Psi\middle|\begin{matrix}(-1,1);(0,1)\\(\Phi-1,1),(-1,1),(-1,1);-\end{matrix}\right], \tag{30}$$

Proof. By definition, the ergodic capacity of a fading channel is given by [5, Eq. (15.21)]

$$\begin{aligned}\overline{C} &= B_w\mathbb{E}\left[\log_2(1+\gamma)\right] \\ &= B_w\int_0^\infty \log_2(1+\gamma) f_\gamma(\gamma)d\gamma.\end{aligned} \tag{31}$$

The logarithmic function can be expressed as an FHF [28, Eq. (8.4.6-5)]

$$\ln(1+\gamma) = H_{2,2}^{1,2}\left[\gamma\middle|\begin{matrix}(1,1),(1,1);-\\(1,1);(0,1)\end{matrix}\right]. \tag{32}$$

Then, substituting (15) and (32) into (31) yields an approximate expression for the ACC as

$$\begin{aligned}\overline{C} \approx &\frac{\Psi B_w}{\Gamma(\Phi)\ln(2)}\frac{1}{2\pi j}\int_{\mathscr{C}_s}\Gamma(\Phi-1+s) \\ &\times\Psi^{-s}\left(\int_0^\infty \gamma^{-s}H_{2,2}^{1,2}\left[\gamma\middle|\begin{matrix}(1,1),(1,1);-\\(1,1);(0,1)\end{matrix}\right]d\gamma\right)ds.\end{aligned} \tag{33}$$

Now, using the Mellin transform (4) of FHF

$$\mathscr{M}_{1-s}\left(H_{2,2}^{1,2}\left[\gamma\left|\begin{matrix}(1,1),(1,1);-\\(1,1);(0,1)\end{matrix}\right.\right]\right)=\frac{\Gamma(2-s)\Gamma^2(s-1)}{\Gamma(s)}, \tag{34}$$

and substituting (34) into (33), (30) is attained, which concludes the proof of *Property 4.2.*

4.2.5 Average symbol error probability

A. Approximate analysis

Property 4.3. The ASEP for several coherent modulation techniques and MRC combiner operating under i.n.i.d GG multipath fading environment can be approximated by

$$\overline{P}_s\approx\frac{\rho\Psi}{\sqrt{\pi}\delta\Gamma(\Phi)}H_{2,2}^{1,2}\left[\frac{\Psi}{\delta}\left|\begin{matrix}(0,1),\left(-\frac{1}{2},1\right);-\\(\Phi-1,1);(-1,1)\end{matrix}\right.\right], \tag{35}$$

where ρ and δ are two parameters depending on the modulation scheme and summarized in Table 2 [29, Table 6.1].

Table 2: Values of ρ et δ for some signaling constellations.

Modulation	M	ρ	δ
BPSK	2	1	2
BFSK	2	1	1
M-PSK	≥ 4	2	$2\sin^2(\pi/M)$
M-FSK	≥ 4	$(M-1)$	1
M-DPSK	≥ 2	2	$4\sin^2(\pi/2M)$
M-QAM	≥ 4	$4-4/\sqrt{M}$	$3/(M-1)$
M-PAM		$2(M-1)/M$	$6/(M^2-1)$

Proof. The ASEP is evaluated as the expectation value of the instantaneous symbol error rate P_s [5, Eq. (8.102)]

$$\overline{P}_s=\int_0^{\infty}P_s(\gamma)f_\gamma(\gamma)d\gamma, \tag{36}$$

where, P_s is the conditional SER of various digital modulations, given by [29, Eq. (6.33)]

$$P_s(\gamma)\approx\rho\mathrm{Q}\left(\sqrt{\delta\gamma}\right), \tag{37}$$

with $Q(.)$ is the Gaussian Q-function defined as [5, Eq. (9.62)]

$$Q(x)=\frac{1}{\pi}\int_0^{\frac{\pi}{2}}e^{-\frac{x^2}{2\sin^2\phi}}d\phi,\ x\geq 0. \tag{38}$$

Substituting (38) into (37) yields

$$P_s(\gamma)\approx\frac{2\rho}{\pi}\int_0^{\frac{\pi}{2}}e^{-\frac{\delta\gamma}{\sin^2\phi}}d\phi,\ \gamma\geq 0. \tag{39}$$

By replacing (39) into (36), the ASEP can be expressed in terms of MGF as

$$\begin{aligned}\overline{P}_s&\approx\frac{2\rho}{\pi}\int_0^{\infty}\left\{\int_0^{\frac{\pi}{2}}e^{-\frac{\delta\gamma}{\sin^2\phi}}d\phi\right\}f_\gamma(\gamma)d\gamma\\&\approx\frac{2\rho}{\pi}\int_0^{\frac{\pi}{2}}M_\gamma\left(-\frac{\delta}{\sin^2\phi}\right)d\phi.\end{aligned}$$

By rewriting the MGF given in (20) in terms of Gamma function, we get an approximate expression of ASEP as

$$\begin{aligned}\overline{P}_s\approx\frac{2\rho\Psi}{\pi\delta\Gamma(\Phi)}\frac{1}{2\pi j}\int_{\mathscr{C}_s}\Gamma(\Phi-1+s)\Gamma(1-s)\left(\frac{\Psi}{\delta}\right)^{-s}\\\times\left\{\int_0^{\frac{\pi}{2}}\sin^{-2s+2}(\phi)\,d\phi\right\}ds,\end{aligned} \tag{40}$$

where $\int_0^{\frac{\pi}{2}}\sin^{-2s+2}(\phi)\,d\phi$ can be expressed, when $\Re(s)<\frac{3}{2}$, in terms of the Beta function [24, Eq. (6.2.1)] as

$$\begin{aligned}\int_0^{\frac{\pi}{2}}\sin^{-2s+2}(\phi)\,d\phi&=\frac{1}{2}B\left(\frac{3}{2}-s,\frac{1}{2}\right)\\&=\frac{\sqrt{\pi}}{2}\frac{\Gamma\left(\frac{3}{2}-s\right)}{\Gamma(2-s)}.\end{aligned} \tag{41}$$

Finally, incorporating (41) into (40), (35) is attained, which concludes the proof of *Property 4.3.*

B. Asymptotic Behavior

Property 4.4. For high SNR values, ASER can be tightly asymptotically approximated as

$$\overline{P}_s=\frac{\rho\Gamma\left(\Phi+\frac{1}{2}\right)}{\sqrt{\pi}\Gamma(\Phi+1)}\left(\frac{\Phi}{\delta}\right)^{\Phi}\overline{\gamma}^{-\Phi}+o\left(\overline{\gamma}^{-\Phi}\right). \tag{42}$$

Proof. Let's rewrite (35) as a Mellin-Barnes integral

$$\begin{aligned}\overline{P}_s(x)\approx\frac{\rho\Psi}{\sqrt{\pi}\delta\Gamma(\Phi)}\frac{1}{2\pi j}\\\times\int_{\mathscr{C}_s}\frac{\Gamma(\Phi-1+s)\Gamma(1-s)\Gamma\left(\frac{3}{2}-s\right)}{\Gamma(2-s)}\left(\frac{\Psi}{\delta}\right)^{-s}ds.\end{aligned} \tag{43}$$

As when $\overline{\gamma}$ tends to infinity, $\frac{\Psi}{\delta}$ approaches to zero, it follows from [32, Theorem 1.11] that (43) can be evaluated as a sum of the residues at the poles located in

LHP, namely at the poles $\{-\Phi-k+1\}_{k\in\mathbb{N}}$ of $\Gamma(\Phi-1+s)$

$$\underset{s=-\Phi-k+1}{\text{Res}}\left[\frac{\Gamma(\Phi-1+s)\Gamma(1-s)\Gamma\left(\frac{3}{2}-s\right)}{\Gamma(2-s)}\left(\frac{\Psi}{\delta}\right)^{-s}\right]$$
$$=\lim_{s\to-\Phi-k+1}(s+\Phi+k-1)\Gamma(\Phi-1+s)$$
$$\times\frac{\Gamma(1-s)\Gamma\left(\frac{3}{2}-s\right)}{\Gamma(2-s)}\left(\frac{\Psi}{\delta}\right)^{-s}.$$

Using the identity $\Gamma(z+1)=z\Gamma(z)$, and

$$\underset{s=-k}{\text{Res}}\,\Gamma(s)=\lim_{s\to-k}(s+k)\Gamma(s)$$
$$=\frac{(-1)^k}{k!},\ (k=0,1,2,\ldots)$$

we have

$$\underset{s=-\Phi-k+1}{\text{Res}}\left[\frac{\Gamma(\Phi-1+s)\Gamma(1-s)\Gamma\left(\frac{3}{2}-s\right)}{\Gamma(2-s)}\left(\frac{\Psi}{\delta}\right)^{-s}\right]$$
$$=\frac{(-1)^k}{k!}\frac{\Gamma\left(\Phi+k+\frac{1}{2}\right)}{\Phi+k}\left(\frac{\Psi}{\delta}\right)^{\Phi+k-1}. \quad (44)$$

and substituting (29) into (44), (42) is deduced. That is, the proof of *Property 4.4.* is concluded.

5 Simulation Results

In this part, the FHF were evaluated using Mathematica software. All the analytical expressions derived are validated using Matlab software via Monte-Carlo simulations, as shown in **Algorithm** 1, by generating 10^7N generalized Gamma distributed random numbers. Furthermore, the inverse transform sampling method [30] is employed along with the exponential decaying power delay profile with equispaced delays [31]

$$\mu_1^{(z_i)}=\mu_1^{(z_1)}e^{-\varphi(i-1)},\ \forall i\in\{1,\ldots,N\}$$

where φ stands for the average power decay factor.

In Fig. 2, the tightness of the proposed approximate PDF is obviously observed over the entire range of z for $e^{-\varphi}=\{1,0.9\}$, $m=2$, $\beta=3$, and different values of N (N = 10, 25, 50). One can see that the greater N is, the curves shift to the right. This is because the greater N is, the greater μ_1 is. Consequently, the maximum value of the probability is attained around such an average. Moreover, based on the KLD criterion, we measure the dissimilarity of the proposed approximate PDF f_Z with respect to the exact one g_Z.
With the aid of the relative entropy (criterion of KLD) defined as [33]

$$D_{KLD}(g_Z\|f_Z)=\int_0^\infty g_Z(x)\log\left\{\frac{g_Z(x)}{f_Z(x)}\right\}dx. \quad (45)$$

Algorithm 1: Evaluate PDF for the sum of i.n.i.d GG RVs

Function cpt=PDF_sum_GG ($m,\beta,\varphi,N,\mu_1^{(z_1)},Max\_z$)
  // $m=\{m_i\}$ and $\beta=\{\beta_i\}$.
  $step\leftarrow 0.01$;
  $z\leftarrow 0:step:Max\_z$; // z range.
  $nb\_generated\_values\leftarrow 10^7$; // generating and ranking (in descendent order) of GG-distributed random values.
  $n\leftarrow length(z)$;
  $cpt^{(0)}\leftarrow 0$; // initialize the PDFs of all range's values to zero.
  for $k\leftarrow 1$ ***to*** $nb\_generated\_values$ **do**
    $a\leftarrow 0$;
    for $i\leftarrow 1$ ***to*** N **do**
      $a\leftarrow a+$ **gengamrand**$(1,m_i*\beta_i/2,\beta_i/2,(\mu_1^{(z_1)}*e^{-\varphi(i-1)}*\Gamma(m_i))/\Gamma(m_i+2/\beta_i))$; //**gengamrand** generates random numbers for the GG distribution.
    end
    if $a\geq 0$ *and* $a\leq Max\_z$ **then**
      $l\leftarrow floor\left(\frac{a}{step}\right)$;
      $cpt^{(l+1)}\leftarrow cpt^{(l+1)}+1$;
    end
  end
  for $l\leftarrow 1$ ***to*** n **do**
    $cpt^{(l)}\leftarrow cpt^{(l)}/nb\_generated\_values/step$;
  end
  return cpt;
end

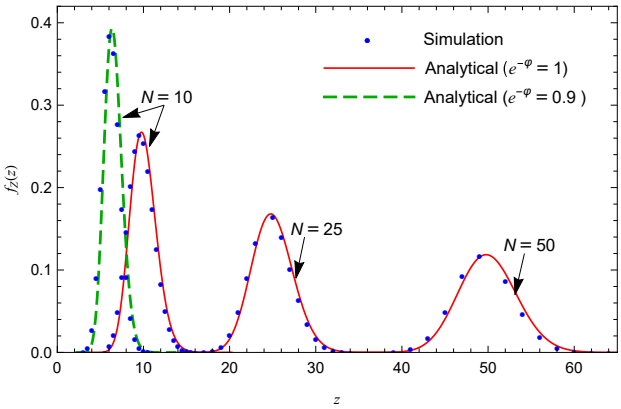

Fig. 2: PDF of i.n.i.d GG sums for $m=2$, $\beta=3$ and various values of N, and φ.

Note that if $D_{KLD}(g_Z\|f_Z)=0$, then $f_Z=g_Z$.

Table 3 presents the degree of similarity between the proposed approximate PDF f_Z and the exact one g_Z using (45) for various values of N. One can see that all numerical

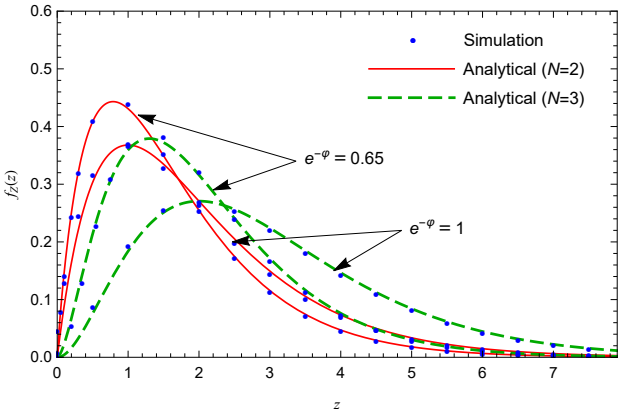

Fig. 3: Approximated and simulated PDF of the sum of GG RVs for ($m = 1$ and $\beta = 2$).

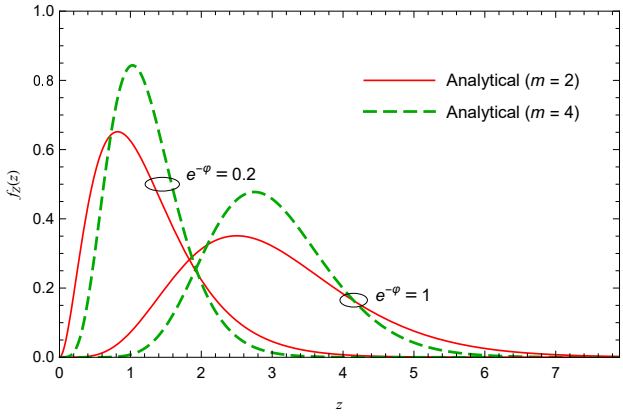

Fig. 4: Analytical PDF of the sum of three GG RVs for $\beta = 2$.

results of KLD are smaller, which corroborates accuracy of our analysis.

Table 3: KLD's measurement for $\varphi = 0$, $m = 2$, and $\beta = 3$.

N	10	25	50
KLD	0.1527	0.1465	0.0331

In Fig. 3, the approximated and the simulated PDF of sum i.n.i.d GG RVs, Z, are plotted using (12) and via Monte-Carlo simulation with the help of **Algorithm 1** over the z's range $[0,8]$. It can be observed that the proposed approximation is tight for all values of φ and N, validating the accuracy of (12). Moreover, the greater φ and N are, the greater μ_1 is. On the other hand, according to (12) related to λ term of lemma 2, and from the condition convergence (11), the value of λ is chosen to be greater than the maximum value of $\triangle$ computed for $m = 1$, $\beta = 2$, and $\varphi = \{0, -\ln(0.65)\}$ (i.e., $\triangle = 4.73$ for $N = 2$ and $\triangle = 6$ for $N = 3$).

In Fig. 4, the approximated PDF versus z is plotted from (12) for $N = 3$, $\varphi = \{0, -\ln(0.2)\}$, $m = \{2,4\}$, and $\beta = 2$. PDF becomes more narrow and close to 1 at $\mu_1 = z$ with the increase of m.

Fig. 5 shows both approximated and simulated CDF computed for $N = 4$, $m = 3$, $\beta = \{1,3\}$, and $e^{-\varphi} = \{1, 1.2\}$. It is noticeable that the curves match well over the entire range. Moreover, the KS statistical test [34] measured for $N \leq 50$, $e^{-\varphi} = \{1, 1.2\}$, $m = 3$, $\beta = 3$, and a given significance level 0.05 shows that the goodness-of-fit calculated by averaging 15 results obtained for 300 samples remains less than the associated critical level 0.0785196, for which the null hypothesis is not rejected, i.e. the approximate CDF is asserted by the data obtained by simulation.

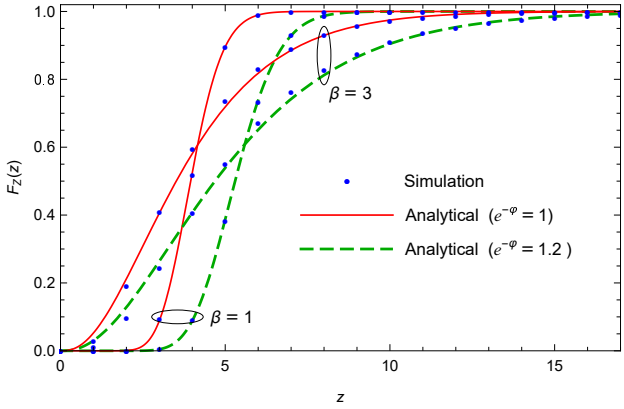

Fig. 5: CDF of i.n.i.d GG sums for $N = 4$ and $m = 3$.

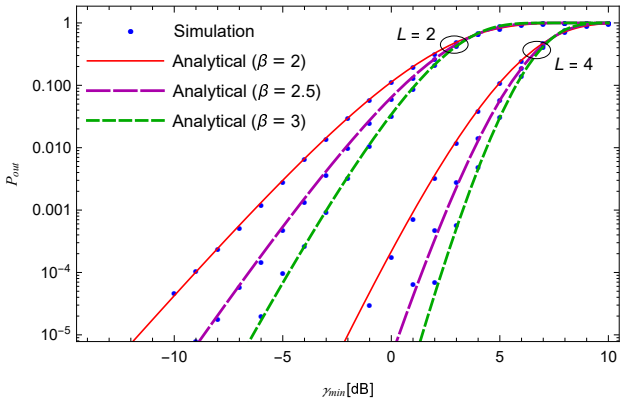

Fig. 6: OP for L-branch receiver and $m = 2$.

Fig. 6 depicts both the approximate and simulated outage probability P_{out} versus γ_{min} (in dB) for $m = 2$, $\varphi = -\ln(1.2)$, and different values of β and L. It is evident that the analytical result, evaluated using (25), are highly accurate with its simulation counterpart.

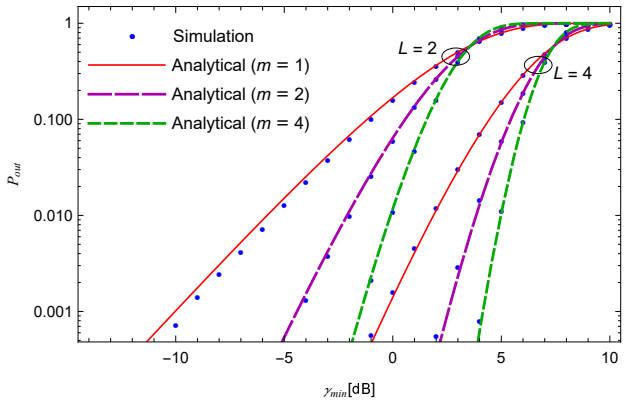

Fig. 7: OP vs minimum SNR for L-branch MRC receiver and $\beta = 2.5$.

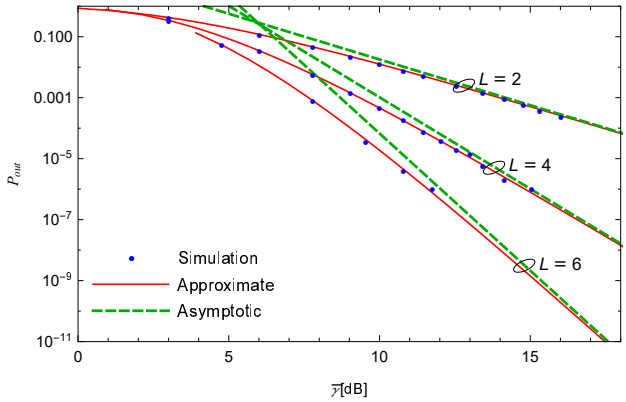

Fig. 8: OP vs average SNR for L-branch MRC, $m = 1.5$, $\beta = 2$, $e^{-\varphi} = 1$ and $\gamma_{min} = 2$dB over i.i.d GG fading channels.

Furthermore, it can be seen that the decrease in OP can be achieved by increasing either L or β, for which the system becomes more reliable.

Fig. 7 shows the evolution of OP versus minimum SNR threshold γ_{min} [dB], plotted from (25) for $\beta = 2.5$, L-branch MRC combiner, and various values of m. Evidently, the greater both the diversity order L and the fading severity m are, the smaller OP is, leading to more reliable system.

The OP of a MRC system is depicted in Fig. 8 over i.i.d GG fading with $m = 1.5$, $\beta = 2$ and $\gamma_{min} = 2$ dB. The approximate expression (25), the asymptotic expression (27), and simulation results are presented. It is observed that simulation results match the approximate expression (25), and that (27) is a high tight upper bound of (25) at high SNRs, which confirms the diversity order.

In both Fig. 9 and Fig. 10, the analytical AoF, given in (24), is plotted as a function of the shape parameter β, for various values of φ, L, and m. It is noticeable that η_γ decreases as β and/or m, L, and the average SNR $\overline{\gamma}_i$ per

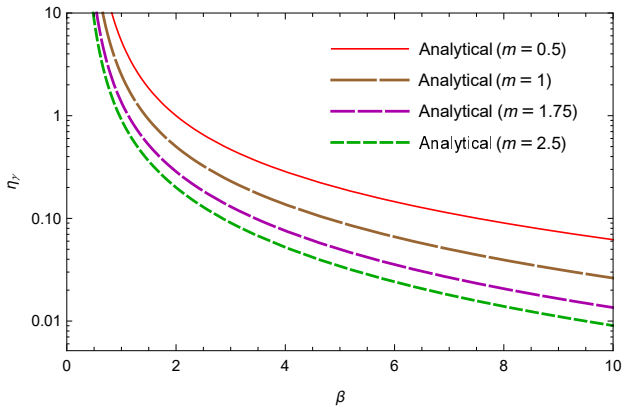

Fig. 9: AoF as a function of β for MRC combiner.

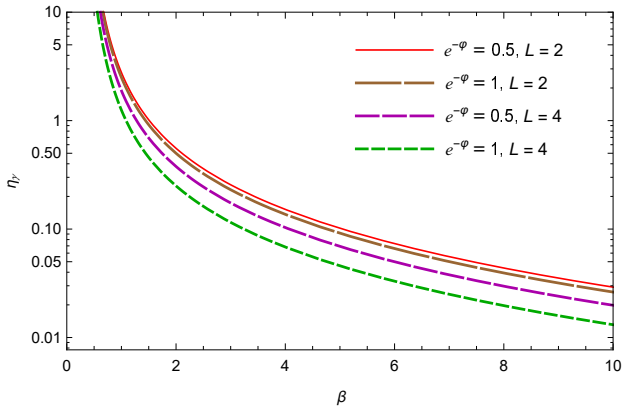

Fig. 10: AoF vs β for $m = 1$.

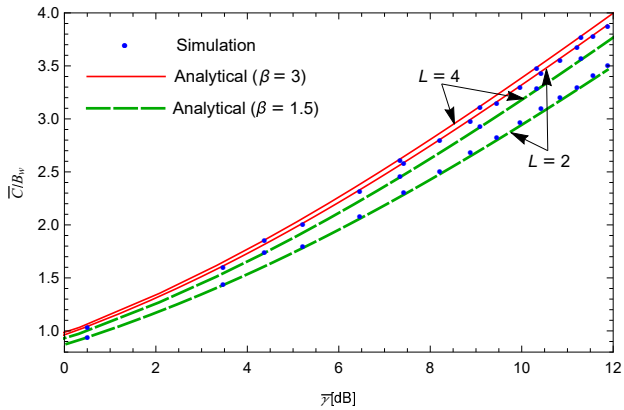

Fig. 11: Normalized ACC vs total average SNR at the output of L-branch MRC receiver for $m = 1$.

branch increase, proving an enhancement of the system performance.

The approximate, and the simulated normalized ACC per bandwidth versus average output SNR, $\overline{\gamma}$, are depicted

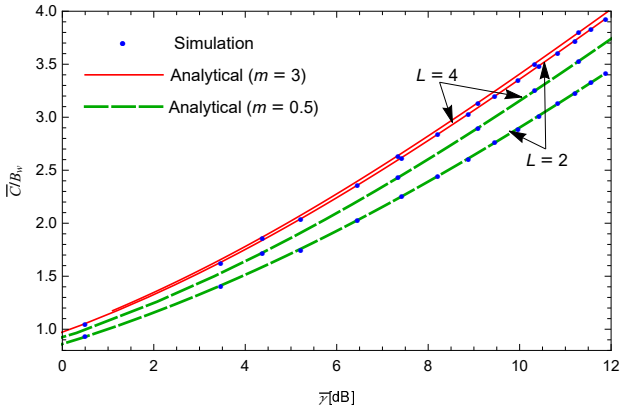

Fig. 12: Normalized ACC vs total average SNR at the output of L-branch MRC receiver for $\beta = 2$.

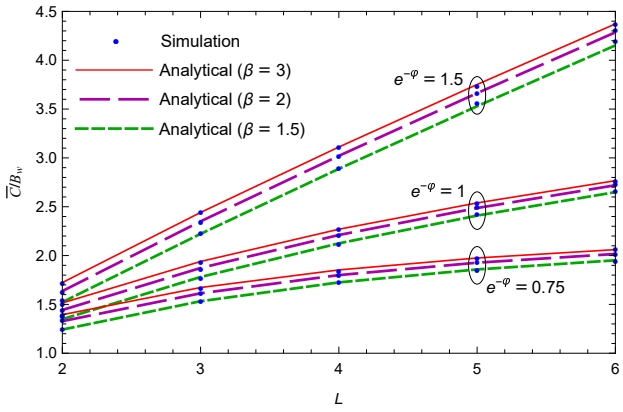

Fig. 13: Normalized ACC vs L for $m = 1$.

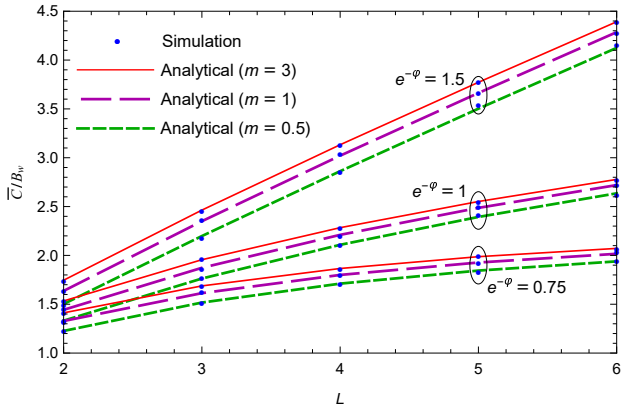

Fig. 14: Normalized ACC vs L for $\beta = 2$.

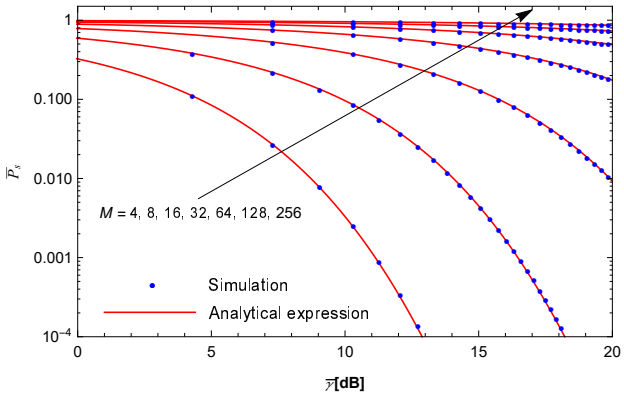

Fig. 15: ASEP for M-PSK modulation scheme vs $\overline{\gamma}$ for $L = 4$, $m = 2$, and $\beta = 3$.

in Fig. 11, plotted using (30), and (31), respectively, for two- and four-branch MRC receiver, and $e^{-\varphi} = 1.2$. The average SNR of signal at the first branch's input $\overline{\gamma}_1$ varies between -6.57 dB and 11.87 dB, and between -2.7 dB and 15.74 dB for $L = 2$ and 4, respectively. One can notice that the ACC increases as $\overline{\gamma}$, β, and L increase. Also, the greater L is, the greater the maximal spectral efficiency of the system is.

Fig. 12 depicts both the analytical and the simulated normalized ACC as a function of average output SNR for two- and four-branch MRC receiver, and $e^{-\varphi} = 1.2$. $\overline{\gamma}_1$ was chosen in $[-2.7\text{dB}, 15.74\text{dB}]$ and $[-6.57\text{dB}, 11.87\text{dB}]$ for $L = 2$ and 4, repectively. The approximate analytical expression for ACC matches the simulated one for different settings of the system parameters. Moreover, it is noteworthy that the ACC is monotonically increasing with the increase of $\overline{\gamma}$, m, and L, leading to a system quality improvement.

In Fig. 13, both the approximate and simulated ACC per bandwidth versus L are plotted for $m = 1$, and various values of β and φ. It is noticeable that both curves match various configuration settings. Also, the greater both the diversity order L and the fading severity β are, the better ACC is.

Fig. 14 illustrates both approximate and simulated ACC per bandwidth versus L for $\beta = 2$, and various values of m and φ. Again, both curves are perfectly matching, which proves accuracy of our result.

Fig. 15 plots the analytical expression and simulated ASEP versus the average SNR at the MRC output from (35) and (36), respectively, for $L = 4$, $e^{-\varphi} = 1.2$, and different values of M, with the help of Table 2. One can notice that the analytical results match the simulated ones. The branch average SNR $\overline{\gamma}_1$ varies between -12.7 dB and 20.3 dB. The smaller M is, the smaller ASEP is. Also, ASEP decreases with the increase of $\overline{\gamma}$, leading to system quality enhancement.

In Fig. 16, the analytical ASEP $\overline{P}_s$ is plotted, from (35), as a function of $\overline{\gamma}$, for BDPSK modulation scheme, based on Table 2, $\beta = 3$, and several values of m and L. ASEP reduces with the increase of $\overline{\gamma}$. Furthermore, system performance improves with the increase of both diversity order L and fading severity m.

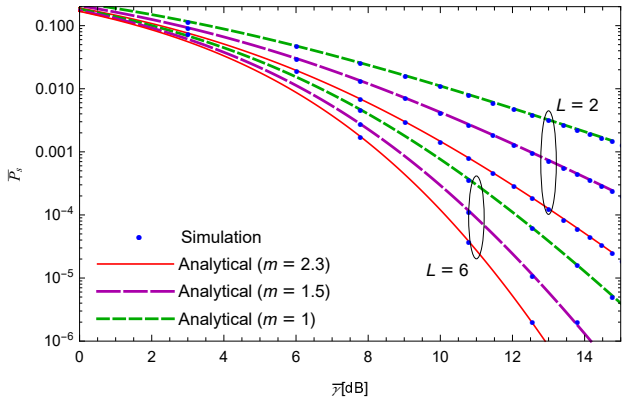

Fig. 16: ASEP for BDPSK modulation technique vs $\overline{\gamma}$ for $\beta = 3$, $\varphi = 0$, and two values of L.

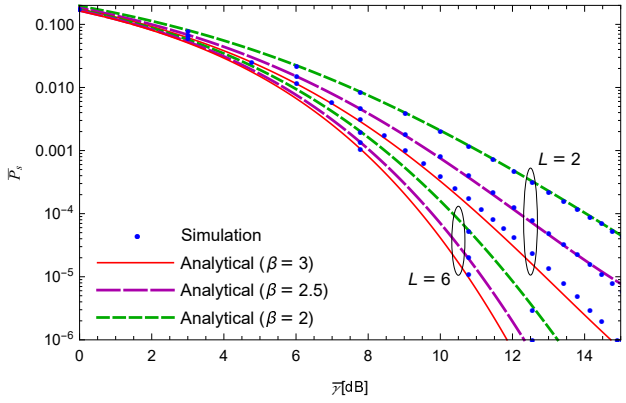

Fig. 17: ASEP vs $\overline{\gamma}$ for BDPSK, $m = 2$, $\varphi = 0$, and two values of L.

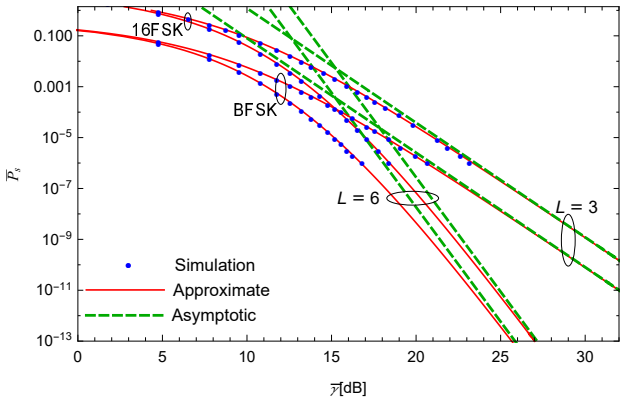

Fig. 18: ASEP as a function of $\overline{\gamma}$ for $m = 1.5$, $\beta = 2$, $\varphi = 0$, and various values of L.

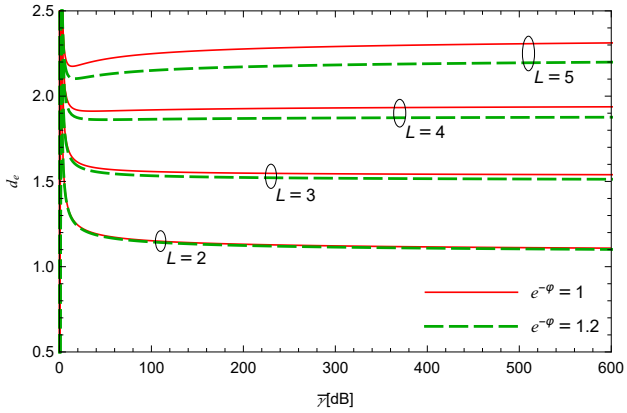

Fig. 19: EDF as a function of $\overline{\gamma}$ for L-branch MRC with BPSK modulation, $m = 0.5$, and $\beta = 2$.

Fig. 17 presents both the approximate and simulated ASEP $\overline{P}_s$ as a function of $\overline{\gamma}$, is plotted for BDPSK modulation, $m = 2$, and several values of β, and L. Again, the greater both L and β are, the smaller the ASEP is.

Fig. 18 compares the approximate expression plotted using (35), the asymptotic (42), and the simulated one for identical L-branch MRC receiver, $m = 1.5$, $\beta = 2$, and both BFSK and 16-FSK modulation scheme. The analytical results (35) match the simulation ones. It is also shown that (35) asymptotically approaches (42) at high SNRs, which achieve the diversity order.

In Fig. 19, the effective diversity order (EDO) is plotted versus $\overline{\gamma}$ for various values of L, $m = 0.5$, $\beta = 2$, and $e^{\varphi} = \{1, 1.2\}$ assuming BPSK modulation scheme relying on the following expression [35]

$$d_e = -\frac{\log \overline{P}_s}{\log \overline{\gamma}}.$$

Then, the asymptotical diversity order (ADO) is given by

$$\lim_{\overline{\gamma} \to \infty} d_e = d_a.$$

Therefore, it is easy to observe from (42) that the diversity order of Φ can be achieved for MRC receiver subject to i.n.i.d GG fading channels. ADO for both $e^{\varphi} = 1$ and $e^{\varphi} = 1.2$ approaches 1, 1.5, 2, and 2.5 as predicted from (42). Moreover, Fig. 19 proves that the convergence of EDO to ADO is slow for i.n.i.d MRC GG fading channels (i.e., $e^{\varphi} = 1.2$) unlike i.i.d MRC GG model (i.e., $e^{\varphi} = 1$).

Table 4: Achievable diversity order for $\varphi = 0$, $m = 0.5$, and $\beta = 2$.

L	2	3	4	5
Φ	1	1.5	2	2.5
d_e	1.09785	1.53333	1.94808	2.34903

Table 4 shows that a diversity order of $\Phi = \{1, 1.5, 2, 2.5\}$ is achieved for L-branches over GG

fading channels emphasizing (42), which means $d_e \sim \Phi$ as $\overline{\gamma} \to \infty$.

6 Conclusion

New accurate approximate expressions for the PDF, and CDF of i.n.i.d GG RVs sums were derived in this paper. The two proposed expressions were validated with the help of KLD criterion and KS test, respectively. Moreover, such tightness was proved by performing their simulation. A perfect match between the approximate expressions and simulate ones was observed. This approach serves the field of wireless communications where the sum of RVs' distribution is necessary for performance metrics evaluation purposes. Accurate approximations for MRC receiver performance criteria experiencing GG fading models, such as OP, ACC, and ASEP have been derived. To gain further insight into the system performance, asymptotic closed-form expressions for the ASEP and OP are further derived and reveal the achievable diversity order for high SNR values.

Acknowledgement

The authors are grateful to the anonymous referee for the careful checking of the details and the constructive comments that improved this paper.

Conflict of interest

The authors declare that there is no conflict of interest regarding the publication of this paper.

References

[1] C. Fox, The *G* and *H*-functions as symmetrical Fourier kernels, *Trans. Amer. Math. Soc.*, **98**, 395-429 (1961).

[2] R. K. Saxena, R. Saxena and S. L. Kalla, Computational solution of a fractional generalization of the Schrödinger equation occurring in quantum mechanics, *Applied Mathematics and Computation*, **216**, 1412-1417 (2010).

[3] A. Mathai, R. K. Saxena, and H. Haubold, *The H-Function: Theory and Applications*, Springer, New York, (2010).

[4] F. Yilmaz and M. S. Alouini, A novel unified expression for the capacity and bit error probability of wireless communication systems over generalized fading channels, *IEEE Trans. Commun.*, **60**, 1862-1876 (2012).

[5] M. Simon and M. S. Alouini, *Digital Communication Over Fading Channels*, 2nd ed., ser. Wiley Series in Telecommun. and Signal Process, Wiley, New York, (2005).

[6] A. J. Coulson, A. G. Williamson, and R. G. Vaughan, *Improved fading distribution for mobile radio*, in IEE Proc.-Commun., **145(13)**, 197-202, (1998).

[7] J. Griffiths and J. P. McGeehan, Interrelationship between some statistical distributions used in radio-wave propagation, IEE Proc. F - Commun., *Radar and Signal Process.*, **129(6)**, 411-417 (1982).

[8] E. W. Stacy, A generalization of the Gamma distribution, *The Ann. Math. Statist.*, **33(3)**, 1187-1192 (1962).

[9] F. El Bouanani and D. B. da Costa, Accurate Closed-Form Approximations for the Sum of Correlated Weibull Random Variables, *IEEE Wirel. Commun. Lett.,* **7(4)**, 498-501 (2018).

[10] F. El Bouanani and H. Ben-azza, Unified analysis of EGC diversity over Weibull fading channels, *Int. Journal of Commun. Syst.*, (2015).

[11] F. El Bouanani, *A new closed-form approximations for MRC receiver over non-identical Weibull fading channels*, in Proc. Int. Wirel. Commun. and Mob. Comp. Conf. (IWCMC), 600-605, (2014).

[12] T. Chaayra, F. El Bouanani and H. Ben-azza, Asymptotic capacity analysis under different adaptive transmission for TAS/MRC MIMO scheme subject to Weibull fading channels, *Physical Communication*, **36**, 100743 (2019).

[13] M. D. Springer, *The Algebra of Random Variables*, Wiley, New York, (1979).

[14] C. D. Bodenschatz, *Finding an H-function distribution for the sum of independent H-function variates*, Ph. D. thesis, University of Texas, Austin, (1992).

[15] H. Jacobs, J. W. Barnes, I. D. Cook, Applications of the H-Function Distribution in Classifying and Fitting Classical Probability Distributions, *American Journal of Mathematical and Management Sciences,* **7**, 131-147 (1987).

[16] I. D. Cook, *The H-Function and probability density functions of certain algebraic combinations of independent random variables with H-function probability distribution*, Ph. D. thesis, University of Texas at Austin, (1981).

[17] V. A. Aalo, G. P. Efthymoglou, T. Piboongungon, C. D. Iskander, Performance of diversity receivers in generalised Gamma fading channels, *IET Commun.,* **1(3)**, 341-347 (2007).

[18] N. C. Sagias, and P. T. Mathiopoulos, Switch diversity receivers over generalized Gamma fading channels, *IEEE Commun. Lett.,* **9(10)**, 871-873 (2005).

[19] P. S. Bithas, N. C. Sagias and T. A. Tsiftsis, Performance analysis of dual-diversity receivers over correlated generalised Gamma fading channels, *IET Commun.,* **2(1)**, 174-178 (2008).

[20] V. A. Aalo, T. Piboongungon, and C. D. Iskander, Bit-Error Rate of Binary Digital Modulation Schemes in Generalized Gamma Fading Channels, *IEEE Commun. Lett.,* **9(2)**, 139-141 (2005).

[21] J. Cheng, T. Berger, *Performance analysis for MRC and postdetection EGC over generalized gamma fading channels*, in Proc. wirel. commun. and net. conf. (WCNC), 120-125, (2003).

[22] N. C. Sagias, P. T. Mathiopoulos, P. S. Bithas and G. K. Karagiannidis, *On the Distribution of the Sum of Generalized Gamma Variates and Applications to Satellite Digital Communications*, in Proc 2nd Int. Symp. on Wirel. Commun. Sys., 785-789, (2005).

[23] N. C. Sagias, G. K. Karagiannidis, P. T. Mathiopoulos and T. A. Tsiftsis, On the performance analysis of equal-gain diversity receivers over generalized gamma fading channels, *IEEE Trans. on Wirel. Commun.,* **5(10)**, 2967-2975 (2006).

[24] M. Abramowitz and I. A. Stegun, *Handbook of mathematical functions with formula graphs and mathematical tables*, National Bureau of Standards, Applied Mathematical Series, (1964).
[25] E. W. Stacy, and G. A. Mihram, Parameter Estimation for a Generalized Gamma Distribution, *Technometrics,* **7(3)**, 349-358 (1965).
[26] T. Chaayra, H. Ben-azza, and F. El Bouanani, A closed-form approximation to the distribution for the sum of independent non-identically generalized gamma variates and applications, *submitted to journal of Mathematical Modelling of Engineering Problems*, (2020).
[27] A. Dadpaya E. S. Soofi R. Soyer, Information measures for generalized gamma family, *Journal of Econometrics,* **138(2)**, 568-585 (1965).
[28] A. P. Prudnikov, Y. A. Brychkov, O. I. Marichev, *Integrals and series, more special functions*, **3**, Gordon and Breach Science, New York, (1990).
[29] A. Goldsmith, *Wireless communications*, Cambridge University Press, (2005).
[30] R.G. Bettinardi, (2017), getKullbackLeibler(P,Q), available at: https://www.mathworks.com/matlabcentral/fileexchange/62981-getkullbackleibler-p-q, MATLAB Central File Exchange. (accessed 19 April 2020).
[31] N. Kong, L. B. Milstein, SNR of generalized diversity selection combining with nonidentical Rayleigh fading statistics, *IEEE Trans. on Commun.,* **48**, 1266-1271 (2000).
[32] A. Kilbas, *H-Transforms, Theory and Applications*, 1st edn., Analytical Methods and Special Functions, Taylor and Francis, (2004).
[33] S. Kullback and R. A. Leibler, On information and sufficiency, *Ann. Math. Statist.,* **22(1)**, 79-86 (1951).
[34] J. Frank, Jr. Massey, The Kolmogorov-Smirnov Test for Goodness of Fit, *Journal of the American Statistical Association,* **46(253)**, 68-78 (1951).
[35] M. Uysal, Diversity analysis of space-time coding in cascaded Rayleigh fading channels, *IEEE Commun. Lett.*, **10(3)**, 165-167 (2006).

Toufik Chaayra received his B.Sc. degree in mathematical sciences and its applications from the Faculty of Sciences, Moulay Ismail University of Meknes, Morocco, in 2009 and M.Sc. degree in applied mathematics and software engineering from the Faculty of Sciences, Abdelmalek Essaadi University of Tetouan, Morocco, in 2011, where he is currently pursuing the Ph.D. degree at the ENSAM, College of Engineering, Moulay Ismail University, Meknes. He has authored various publications in international conferences and journals such as Elsevier, IEEE ACOSIS, ACM ICSDE. His main research interests include analytical statistics, mathematical modeling, information theory, and performance analysis of wireless communication systems.

Hussain Ben-azza is a Professor at ENSAM-National High School of Arts and Trades, Meknes, Morocco, attached to Department of Industrial and Production Engineering, Moulay Ismail University. He obtained his Ph.D. degree in mathematics and computer science in 1995 from Claude Bernard University Lyon 1, France. His research interests include coding theory, cryptography, wireless communications, but also applications of optimization techniques to industrial engineering.

Faissal El Bouanani was born in Nador, Morocco, in 1974. He received the M.S. and Ph.D. degrees in network and communication engineering from Mohammed V Souissi University, Rabat, Morocco, in 2004 and 2009, respectively. He served as a Faculty Member with the University of Moulay Ismail, Meknes, from 1997 to 2009, before joining the National High School of IT/ENSIAS, College of Engineering, Mohammed V University, Rabat, in 2009, where he is currently an Associate Professor. His current research interests include coding, cryptography, and performance analysis of wireless communication systems. His Ph.D. thesis was awarded the Best One by Mohammed V-Souissi University, in 2010.

Dr. El Bouanani advised multiple Ph.D. and masters degree students at Mohammed V University and Moulay Ismail University. His research efforts have culminated in more than fifty articles in a wide variety of international conferences and journals, including the IEEE T RANSACTIONS ON COMMUNICATIONS, IEEE ACCESS, the IEEE WIRELESS COMMUNICATIONS LETTERS, the IEEE TRANSACTIONS ON SUSTAINABLE COMPUTING, the *Eurasip Journal on Wireless Communications and Networking*, the *Wiley International Journal of Communication Systems*, *Physical Communication Journal*, PIMRC, GLOBECOM, IWCMC, and CROWNCOM. He served as the TPC Chair for ICSDE conferences and the General Co-Chair of ACOSIS'16 and CommNet'18 conferences. He has been involved also as a TPC Member in various conferences, including VTC, ISWCS, IWCMC, UNET, and WINCOM. He served as the General Chair for 2019 and 2020 CommNet conference, as well as a Reviewer of the IEEE COMMUNICATIONS LETTERS and the IEEE TRANSACTIONS ON COGNITIVE COMMUNICATIONS AND NETWORKING.